JOURNAL OF MATERIALS SCIENCE 19 (1984) 2145–2152

Heat flow model of rapid solidification with nonhomogeneous thermal contact

R. SELLGER, W. LÖSER, W. NEUMANN
Central Institute of Solid State Physics and Materials Research of the Academy of Sciences of GDR, DDR – 8027 Dresden, GDR

A heat flow model is presented of the solidification process of a thin melt layer on a heat conducting substrate. The model is based on the two-dimensional heat conduction equation, which was solved numerically. The effect of coexisting regions of good and bad thermal contact between foil and substrate is considered. The numerical results for thermal parameters of the Al–Cu eutectic alloy show considerable deviations from one-dimensional solidification models. Except for drastic differences in the magnitude of the solidification rate near the foil–substrate interface, the solidification direction deviates from being perpendicular to the substrate and large lateral temperature gradients occur. Interruption of the thermal contact may lead to back-melting effects. A new quantity, the effective diffusion length, is introduced which allows some conclusions to be drawn concerning the behaviour of the frozen microstructure during subsequent cooling.

Nomenclature

$\bar{a}_i, a_i$	Thermal diffusivity $\bar{a}_i = \bar{k}_i/c_i\rho_i$, $a_i = \bar{a}_i/\bar{a}_1$.
c_i	Specific heat capacity.
d	Foil thickness.
D	Solid state diffusion coefficient.
$\mathbf{e}_x, \mathbf{e}_z$	Unit vectors.
H	Latent heat of fusion.
h_α, h_β	Foil-substrate heat transfer coefficients.
i	Index: 1, melt; 2, solidified foil; 3, substrate.
$\bar{k}_i, k_i$	Thermal conductivity $k_i = \bar{k}_i/\bar{k}_1$
$\mathbf{n}$	Normal unit vector.
Nu_α, Nu_β, $Nu(x, \tau)$	Nusselt numbers for regions of bad and good thermal contact, respectively $Nu_\alpha = h_\alpha d/\bar{k}_1$, $Nu_\beta = h_\beta d/\bar{k}_1$, $Nu(x, \tau) = h(x, \tau)\, d/\bar{k}_1$.
R	Universal gas constant.
$\bar{\mathbf{s}}, \mathbf{s}$	Position of the liquid–solid interface $\bar{\mathbf{s}}/d = \mathbf{s} = s_x\mathbf{e}_x + s_z\mathbf{e}_z$.
$\dot{\mathbf{s}}$	Local solidification rate $\dot{\mathbf{s}} = \mathrm{d}\mathbf{s}/\mathrm{d}\tau$.
t	Real time.
T_i	Temperature field.
T_0	Ambient temperature.
T_f	Melting temperature.
u_i	Dimensionless temperature field $u_i(x, z, \tau) = T_i(x, z, \tau)/T_f$.
u_0	Dimensionless ambient temperature $u_0 = T_0/T_f$.
$\dot{u}_i$	Local cooling rate within the foil $\dot{u}_i = \mathrm{d}u_i/\mathrm{d}\tau$.
W	Stefan number $W = H/c_1T_f$.
$\bar{x}, x$	Cartesian coordinate parallel to the foil–substrate interface $x = \bar{x}/d$.
$\bar{x}_0, x_0$	Lateral extension of foil section $x_0 = \bar{x}_0/d$.
$\bar{x}_1, x_1$	Lateral contact length $x_1 = \bar{x}_1/d$.
$\bar{z}, z$	Cartesian coordinate perpendicular to the foil–substrate interface $z = \bar{z}/d$.
$\bar{z}_0, z_0$	Substrate thickness $z_0 = \bar{z}_0/d$.
ΔE	Activation energy of diffusion.
ΔT	Initial superheat of the melt.
Δu	Dimensionless initial superheat $\Delta u = \Delta T/T_f$.
$\theta(x)$	Step function $\theta(x) = \begin{cases} 0 & x < 0 \\ 1 & x \geqslant 0. \end{cases}$ if
λ_{eff}	Dimensionless effective diffusion length.
ρ_i	Mass density.
τ	Dimensionless time $\tau = t\bar{a}_1/d^2$.
$\tau_f, \tau_f(x, z)$	Total and local dimensionless freezing time, respectively.

0022–2461/84 $03.00 + .12

TABLE I Thermophysical properties

Description	Property						
	c(J kg^{-1} K^{-1})	H(J kg^{-1})	T_f(K)	k(Wm^{-1} K^{-1})	ρ(kg m^{-3})	D_0(m^2 sec^{-1})	ΔE(kJ mol^{-1})
Foil*(Al–Al_2Cu)	779	3.42×10^{-5}	821	88.8	3.30×10^3	2.3×10^{-4}	146
Substrate (Cu)	331	–	–	329	8.93×10^3	–	–

*Unified parameters for liquid and solid state

1. Introduction

Rapid quenching of metallic alloys directly from the melt has attracted much attention because of the large potential for new material properties originating in the refinement of the cast structure, extended solid solubility, metastable crystalline phases and amorphous alloys [1]. The various experimental set-ups are based on bringing the liquid metal in intimate contact with a massive chill-block (see [2] for a comprehensive review). Because of the high cooling rates realized it is difficult to measure the relevant process parameters. Therefore attempts have been made to calculate the operating conditions for the formation of crystalline and amorphous foils from heat flow models. The liquid–solid interface velocity [3–5] and the cooling rate [5–7] were calculated. In all of these models a homogeneous heat transfer between foil and substrate was supposed. Recently the role of ribbon-wheel wetting pattern in the melt spinning process, its dependence on some process parameters and its effect on morphology of the amorphous ribbon and effective heat-transfer coefficient was studied experimentally [8–10].

In this paper a theoretical model is presented for the solidification and subsequent cooling of a crystalline foil on a metallic substrate taking into account the locally inhomogeneous foil–substrate contact by means of different heat-transfer coefficients. The parameters for the Al–17.3 at% Cu eutectic alloy (see Table I) were used in the numerical calculations, because this alloy has already been the subject of several experimental investigations [10–15].

2. Mathematical model

The solidification model of a thin foil on a heat conducting substrate is illustrated in Fig. 1. The model considers general features of the rapid solidification process and is not restricted to a special technique. In case of the continuous melt spinning process [8], the model can be applied in the sense that the origin of the coordinate system is fixed on the ribbon and the curvature of the substrate surface is neglected within the length of ribbon considered.

The effect of coexisting regions of good and less effective thermal contact to the substrate is included in the expression for the foil-substrate heat transfer function

$$h(x, \tau) = h_\alpha + (h_\beta - h_\alpha)\theta(x - x_1) \quad (1)$$

The two-dimensional heat flow equations with temperature independent material parameters,

$$\frac{\partial u_i}{\partial \tau} = a_i \left(\frac{\partial^2 u_i}{\partial x^2} + \frac{\partial^2 u_i}{\partial z^2} \right) \quad (2)$$

are used in connection with the boundary conditions

$$k_3 \frac{\partial u_3(x, 0)}{\partial z} = Nu(x, \tau)\,[u_2(x, 0) - u_3(x, 0)] \quad (3)$$

at the foil–substrate interface,

$$\frac{\partial u_1(s_x, s_z)}{\partial \mathbf{n}} - k_2 \frac{\partial u_2(s_x, s_z)}{\partial \mathbf{n}} = W \frac{\partial s}{\partial \tau} \quad (4)$$

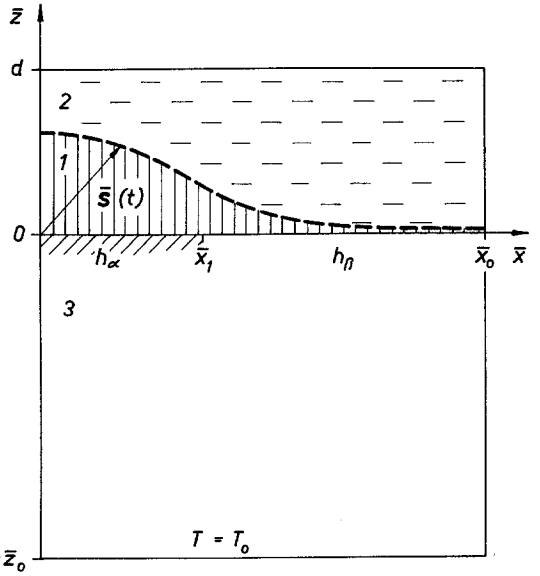

Figure 1 Sketch of the geometry of a freezing melt layer.

at the liquid-solid interface, and

$$\frac{\partial u_1(x,d)}{\partial z} = \frac{\partial u_i(0,z)}{\partial x} = \frac{\partial u_i(x_0,z)}{\partial x} = 0 \tag{5a}$$

$$u_3(x,-z_0) = u_0 \tag{5b}$$

at the outer boundaries, and the initial condition

$$u_1(x,z,0) = 1 + \Delta u \tag{6a}$$

$$u_3(x,z,0) = u_0 \tag{6b}$$

which includes a finite superheat.

The mathematical problem was solved numerically by the explicit finite difference method [16]. The release of the latent heat at the liquid–solid interface s, defined by $u_1\ (s,\tau) = 1$, is treated by an additional procedure.

Although all information on the solidification process is contained in the solution for the temperature fields $u_i(x,z,\tau)$, it is useful to consider some related quantities. In particular, relating the foil microstructure with the characteristics of the solidification process, the local solidification rate, $\dot{s}(x,z)$, and the quantity

$$\lambda_{\mathrm{eff}}(x,z) = \frac{1}{d}\left\{\int_{\tau_f(x,z)}^{\infty} D[u(x,z,\tau)]\,\mathrm{d}\tau\right\}^{1/2} \tag{7}$$

representing an effective diffusion length, should be useful for characterizing the primary structure resulting from the solidification process and its subsequent evolution by solid state diffusion during the cooling process, respectively. An Arrhenius law $D = D_0 \exp(-\Delta E/RT_f u)$ was used for the solid state diffusion coefficient of copper in an α–Al matrix.

3. Numerical results and discussion

3.1. Homogeneous foil–substrate heat transfer ($Nu_\alpha = Nu_\beta$)

In this case the problem is reduced to one dimension and the quantities depend on z only. In Fig. 2 the freezing process of a melt layer is illustrated for a given value of Nu by some characteristic temperature distributions. Within a first stage characterized by relatively high cooling rates $\dot{u}$ in the melt the superheat is reduced. Within the next period essentially the latent heat released at the liquid–solid interface is extracted. Only in the solidified part of the foil considerable temperature gradients occur and $\dot{u}$ has its maximum ahead of the liquid–solid interface. The

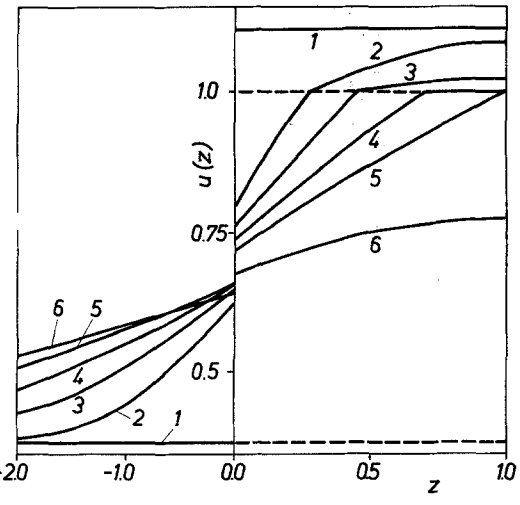

Figure 2 Thermal profile $u(z,\tau)$ of foil and substrate for different times $\tau/\tau_f = 0.0$ (1), 0.13 (2), 0.31 (3), 0.58 (4), 1.00 (5), 1.37 (6) with $Nu = 5.0$ and $\tau_f = 1.42$.

temperature of the melt remains nearly constant. The substrate temperature increases and the discontinuity at the foil–substrate interface is gradually reduced. After completion of the solidification the temperature distribution of the foil becomes more and more smooth and $\dot{u}$ may again increase because of the lack of the latent heat contribution.

The behaviour of the local solidification rate shown in Fig. 3 which differs considerably from the monotonous decrease with z in the case of a semi-infinite layer [5] can be explained on the basis of the different temperature distributions. In particular, the initial rise of $\dot{s}(z)$ is due to the reduction of the steep melt temperature gradient near the substrate introduced by the initial conditions. This part of the plot is sometimes covered in numerical calculations with insufficient accuracy, e.g. in [3]. The decrease of $\dot{s}(z)$ after the maximum which only occurs for high Nusselt numbers is mainly due to the reduced heat transfer because of the increase of the substrate temperature. For large superheat this region can be succeeded by a second maximum of $\dot{s}(z)$ because after the exhaustion of the melt superheat the freezing process is again accelerated. This effect occurs typically for foils of finite thickness. The subsequent range of monotonous decrease of the solidification rate is a consequence of the thermal resistance of the solidified part of the foil and is nearly unaffected by superheat. Generally, increasing Δu and decreasing Nu not only

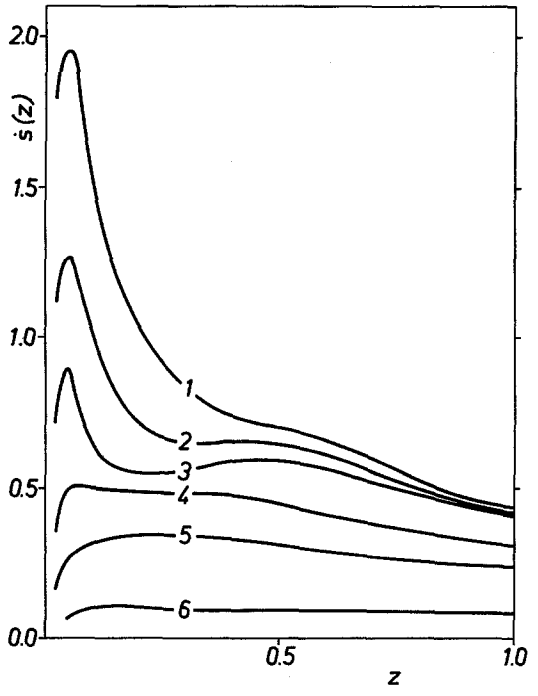

Figure 3 Local solidification rate $\dot{s}(z)$ within the foil with different Nusselt numbers and values of super-heat (1) $Nu = 5.0$, $\Delta u = 0.122$; (2) $Nu = 5.0$, $\Delta u = 0.244$; (3) $Nu = 5.0$, $\Delta u = 0.488$; (4) $Nu = 1.0$, $\Delta u = 0.122$; (5) $Nu = 0.5$, $\Delta u = 0.122$; (6) $Nu = 0.1$, $\Delta u = 0.122$.

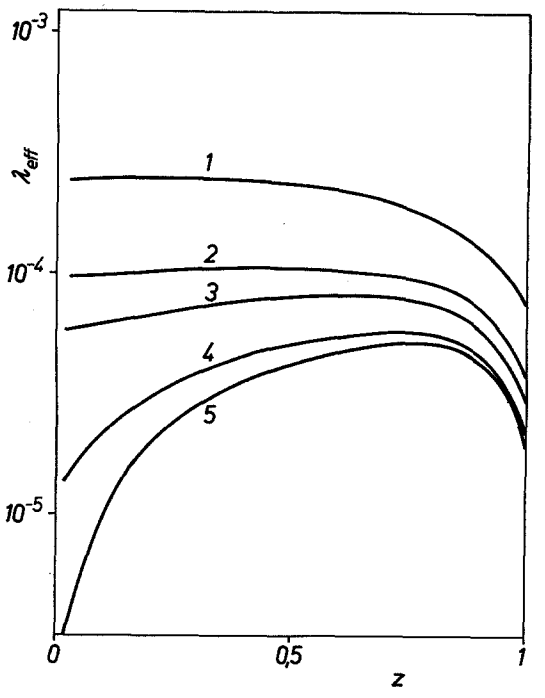

Figure 4 Effective diffusion length λ_{eff} within the foil with different Nusselt numbers (1) $Nu = 0.1$, (2) $Nu = 0.5$, (3) $Nu = 1.0$, (4) $Nu = 5.0$, (5) $Nu = 50.0$.

reduce the solidification rate but also tend to smooth the maximum.

The effective diffusion length λ_{eff} in the solid state is at its minimum at the foil–substrate interface for $Nu \gtrsim 0.5$ because in that part of the foil the temperature after solidification is quickly reduced below the melting point and therefore the solid state diffusion during the cooling process is limited (see Fig. 4). The reduced λ_{eff} near the top surface of the foil on the other hand is due to the fact that this region is the last to be frozen and solid state diffusion acts only for $\tau > \tau_f$. With decreasing Nusselt number the maximum of λ_{eff} is gradually shifted to the foil–substrate interface because the temperature gradients within the foil are reduced and even the solidified part of the foil remains nearly at melting temperature until the freezing process is completed.

3.2. Locally inhomogeneous foil–substrate heat transfer ($Nu_\alpha \neq Nu_\beta$)

The lift-off areas observed at the bottom surface of amorphous as well as crystalline ribbons [8–10] should give rise to a strongly reduced heat transfer (heat radiation or conduction across the air gap) between foil and substrate. Although the accurate values of Nusselt numbers applicable and the configuration of the lift-off areas are unknown, the main effects can be demonstrated by our two-dimensional model supposing some different values of Nu_α and Nu_β.

In Fig. 5 the local solidification rate $\dot{s}$ and the position of the solidification front are shown for a foil with coexisting regions of good and less effective thermal contact. The extent of these regions is typically less than or of the order of the foil thickness. The absolute value of $\dot{s}$ is greatest over the contact area where the soldification direction is perpendicular to the foil–substrate interface. In an extended range of the foil above the lift-off areas, the solidification front advances with a continuously decreasing absolute value of the velocity and an inclined direction because the heat flow is directed to the contact areas. Solidification parallel to the foil–substrate interface of certain foil regions was already concluded from microstructural observations [13, 14]. Near the top surface of the foil the solidification rate vectors are again tilted into the vertical direction. Within a certain range above the lift-off area, situated near the foil surface, the solidification rate is again enhanced. This is connected with the

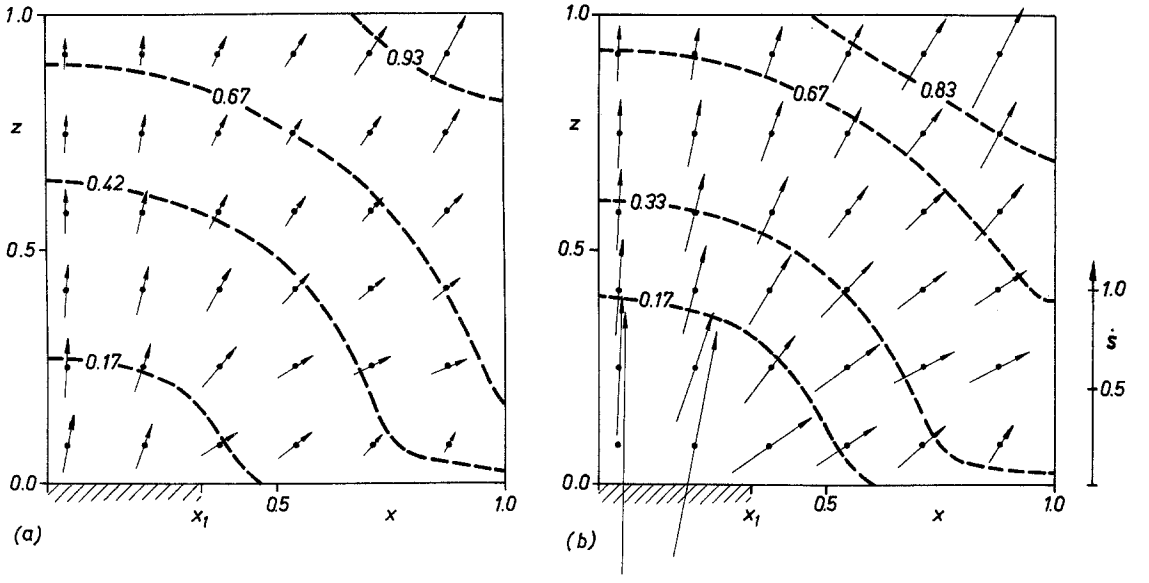

Figure 5 Local solidification rates $\dot{s}(x, z)$ (arrows with lengths proportional to the absolute values of $\dot{s}$) and position of the liquid-solid interface (dashed lines) at characteristic time τ/τ_f in the case of non-homogeneous foil-substrate contact for (a) $Nu_\alpha = 1.0$ (shaded section), $x_1 = 0.3$, $Nu_\alpha/Nu_\beta = 10^2$, $\Delta u = 0.122$, $\tau_f = 5.66$ and (b) $Nu_\alpha = 5.0$, $x_1 = 0.3$, $Nu_\alpha/Nu_\beta = 10^2$, $\Delta u = 0.122$, $\tau_f = 2.88$.

change of the interface shape from concave to convex towards the substrate. Comparing Fig. 5a and b it is seen that the maximum of $|\dot{s}|$ and the freezing time τ_f mainly depend on the maximum Nusselt number Nu_α. The qualitative behaviour is the same for both cases. Only ahead of the thermal contact area is the freezing process comparable with the homogeneous case (see Section 3.1).

In Fig. 6a it is demonstrated that the effective solid state diffusion length λ_{eff} is a minimum near the contact area and in the last solidified region but the maximum is located at the foil centre above the contact area. In the case of extended

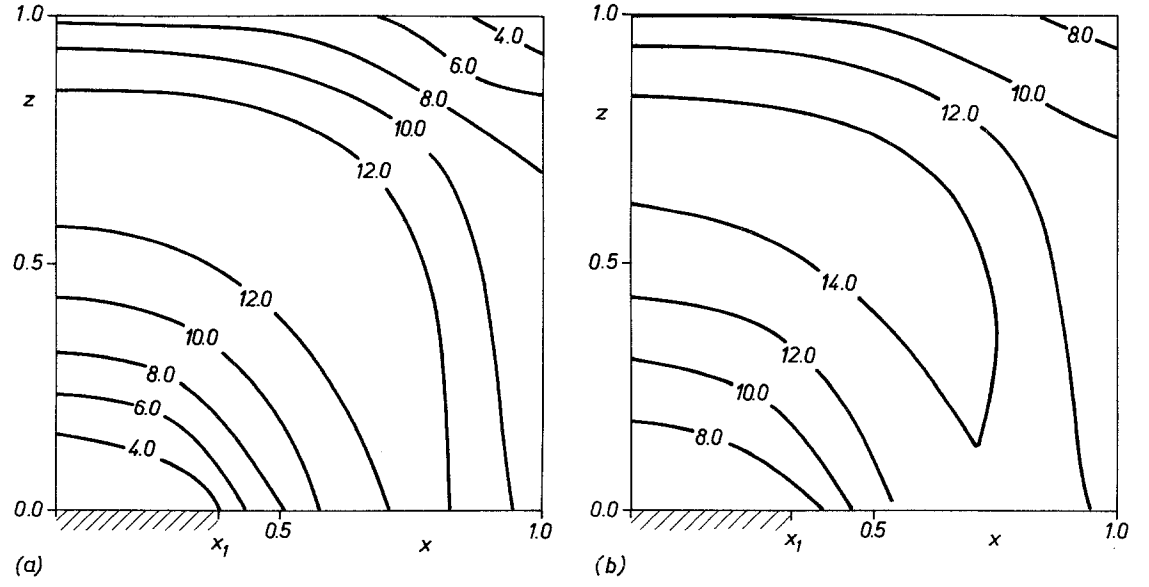

Figure 6 Isolines of effective diffusion length $10^5 \times \lambda_{eff}$ for a set parameters corresponding to Fig. 5b, (a) with permanent contact and (b) with air cooling. $Nu_\alpha = Nu_\beta = 10^{-4}$ at $\tau \geqslant 1.25\ \tau_f$.

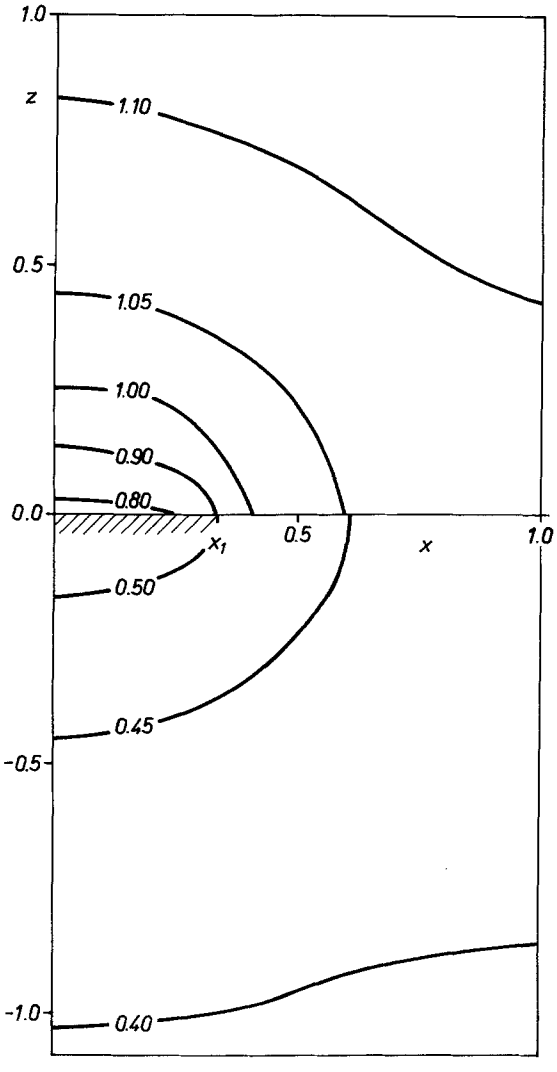

Figure 7 Isotherms at $\tau/\tau_f = 0.16$ within foil and substrate in case of non-homogeneous foil–substrate contact for a set of parameters corresponding to Fig. 5b.

lift-off areas which are large compared with the foil thickness, numerical examples show that the main freezing direction is parallel to the substrate and $|\dot{s}|$ is small far from the thermal contact area. The maximum λ_{eff} occurs above the lift-off areas under those circumstances.

Finally Fig. 7 illustrates the temperature field during the initial stage of the solidification process. The isotherms are curved around the thermal contact areas and gradually become parallel to the foil–substrate interface at distances comparable with the foil thickness. The thermal field implies that at the contact area the coldest part of the foil section is adjoined at the region of maximum substrate temperature and large tangential temperature gradients appear near the boundary of the contact area. In connection with the different thermal expansion coefficients of the foil and substrate this is the origin of large tangential stresses at the foil–substrate interface which could cause the foil to separate from the substrate. In later stages of the solidification process the tangential temperature differences are more and more reduced.

The numerical examples of this section are especially concerned with Nusselt numbers in the range between ideal and Newtonian cooling which are most appropriate for the experiments [6, 18]. The results are given in a compact non-dimensional form. For illustration the following examples of real quantities are presented. In case of $Nu = 5$ (Fig. 5b) one obtains with $d = 40\,\mu m$, the value of $h = 1.1 \times 10^7\,W m^{-2}\,K^{-1}$ corresponding to an upper limit for melt spinning [5], $t_f = 1.34 \times 10^{-4}$ sec, maximum $|\dot{s}| = 1.16\,msec^{-1}$ and maximum $\lambda_{eff} = 4.0 \times 10^{-9}$ m. The latter value means that structural details less than 4 nm are smoothed by diffusion during the cooling process. On the other hand $Nu = 1$ (Fig. 5a) and $d = 2\,\mu m$ leads to $h = 4.4 \times 10^7\,W m^{-2}\,K^{-1}$, $t_f = 2.9 \times 10^{-7}$ sec, maximum $|\dot{s}| = 6.85\,m\,sec^{-1}$ and maximum $\lambda_{eff} = 1.6 \times 10^{-10}$ m.

3.3. Temporal change of the heat transfer

Although the substrate–foil contact in several rapid quenching techniques is expected to change with time, e.g. in the melt spinning process [3], the effect of this phenomenon on the freezing process has not yet been considered. In this section we treat two principal situations for abrupt change of the thermal contact. In Fig. 8 results are represented in a situation where the originally good contact is interrupted before the solidification was complete. As shown the solidification process is not only decelerated but as a consequence of the superheat even backmelting of the solidified part occurs at $0.04 < \tau/\tau_f < 0.12$, before the solidification proceeds further. This leads to abrupt transitions between foil sections which were solidified with completely different rates in the ultimate state of the foil. The observed backmelting phenomenon occurs only if the good contact is lost at a rather early stage of solidification, e.g. 10% of volume was solidified in our example, and for considerable superheat. After the switch-off of the good thermal contact the homogeneous contact case is realized and the

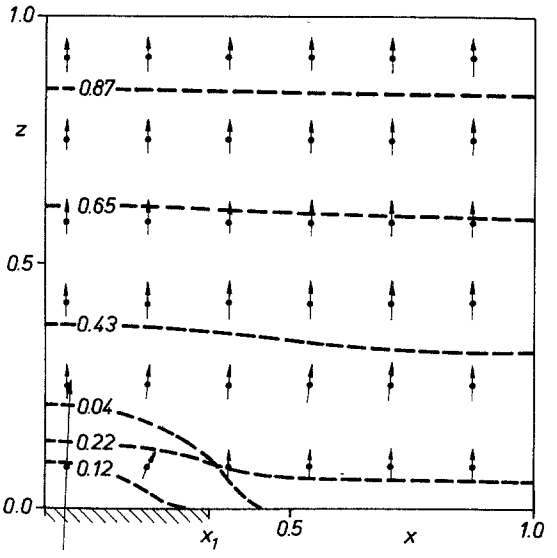

Figure 8 Ultimate solidification rates (arrows) and position of the liquid-solid interface (dashed lines) at characteristic times τ/τ_f in the case of an abrupt loss of good thermal contact at $\tau/\tau_f = 0.04$ with $Nu_\alpha = 5.0, x_1 = 0.3$, $Nu_\alpha/Nu_\beta = 25$, $\Delta u = 0.244$, at $\tau/\tau_f \leqslant 0.04$ and $Nu_\alpha = Nu_\beta = 0.2$ at $\tau/\tau_f > 0.04$, $\tau_f = 6.92$.

solidification front is adjusted to being nearly parallel to the foil-substrate interface.

The other case considered is the loss of good thermal contact after the foil has completely solidified. The foil–substrate heat transfer was replaced at $\tau > \tau_f$ by a Nusselt number characterizing air-cooling. This corresponds to the separation of the ribbon in melt spinning. The calculations show that after a short transient stage during which the temperature differences within the foil are smoothed, the solidified foil is further cooled down with practically homogeneous temperature.

The effect of reducing the solid state cooling rate at $\tau = 1.25\ \tau_f$ on λ_{eff} is shown in Fig. 6b. The effective diffusion length is increased and the local differences are decreased compared with the case of permanent contact (Fig. 6a).

The quantitative effect on λ_{eff} depends very sensitively on the foil–substrate separation time because the average foil temperature rapidly decreases after completion of solidification if the thermal contact is maintained and the diffusion coefficient steeply decreases with temperature (e.g. $D(u = 0.95)/D(u = 0.85) = 14.1$).

In the numerical example the increment of λ_{eff} during the air-cooling stage exceeds the other contributions if the separation time is $\lesssim 1.15\ \tau_f$.

4. Summary and conclusions

The influence of local differences and temporal changes of the foil–substrate heat transfer lead to the following new effects compared with the common one-dimensional heat-flow models for rapid solidification [3, 5–7]:

(a) Large lateral differences of the absolute value of the solidification rate $\dot{s}$ and strong deviations of its direction from perpendicular to the substrate,

(b) convex curvature of the isotherms around the contact area and considerable lateral temperature gradients within foil and chill-block near the boundaries of the contact areas,

(c) local differences of the effective diffusion length λ_{eff} with a minimum near the contact area and a maximum in the central section of the foil,

(d) abrupt changes of the local solidification rate within the foil (under certain circumstances backmelting of the solidified parts of the foil), an increase of the magnitude of the effective diffusion length λ_{eff} and smoothing of its local differences (compared with the case of persistent thermal contact) due to a sudden interruption of the thermal contact.

The main shortcomings of the model are the neglect of melt flow in the heat transport, of kinetic effects at the liquid–solid interface which would, for example, cause the real freezing temperature to be lower than T_f for high solidification rates and the oversimplification of the contact area pattern which does not fully correspond to the experimental observations [8–10]. Nevertheless this model is useful for the interpretation of some microstructural peculiarities connected with the lift-off areas, e.g. at the bottom side of thin melt-spun ribbons of the Al–17.3 at% Cu eutectic alloy [10]. For example over extended lift-off areas (larger than the ribbon thickness) Al- and Al_2Cu-lamellae directed parallel to the ribbon-wheel interface were detected at the bottom side of the ribbon. On the other hand over contact areas localized single phase domains of highly supersaturated α-Al solid solution surrounded by a degenerated microstructure consisting of the two aluminium and Al_2Cu equilibrium phases were found. These observations qualitatively agree with some suggestions made in this paper

concerning the variation of direction and absolute value of the local solidification rate caused non-homogeneous thermal contact.

Acknowledgements

The authors are grateful to Mr Oehm and Dr. Volkmar for help in numerical calculations and Professor Barthel and Dr Jurisch for useful discussions.

References

1. T. R. ANANTHARAMAN and C. SURYANARAYANA, *J. Mater. Sci.* 6 (1971) 1111.
2. H. JONES, "Ultrarapid Quenching of Liquid Alloys" edited by H. Herman (Academic Press, London, 1981) pp. 1–71.
3. P. H. SHINGU and R. OZAKI, *Metall. Trans.* **6A** (1975) 33.
4. K. MIYAZAWA and J. SZEKELY, *ibid.* **10B** (1979) 349.
5. T. W. CLYNE and A. GARCIA, *J. Mater. Sci.* **16** (1981) 1643.
6. R. C. RUHL, *Mater. Sci. Eng.* **1** (1967) 313.
7. H. -W. BERGMANN, H. U. FRITSCH and G. HUNGER, *J. Mater. Sci.* **16** (1981) 1935.
8. S. C. HUANG and H. C. FIEDLER, *Metall. Trans.* **12A** (1981) 1107.
9. *Idem, Mater. Sci. Eng.* **51** (1981) 39.
10. W. NEUMANN, M. LEONHARDT, W. LÖSER and R. SELLGER, to be published.
11. B. PREDEL and G. DUDDEK, *Z. Metallk.* **69** (1978) 773.
12. M. H. BURDEN and H. JONES, *J. Inst. Met.* **98** (1970) 249.
13. D. B. WILLIAMS and J. W. EDINGTON, *J. Mater. Sci.* **12** (1977) 126.
14. K. CHATTOPADHYAY, A. P. RAMIENI and P. RAMACHANDRARAO, *ibid.* **15** (1980) 797.
15. R. K. SINGH, K. CHATTOPADHYAY, S. LELE and T. R. ANANTHARAMAN, *ibid.* **17** (1982) 1617.
16. M. G. SALVADORI and M. L. BARON, "Numerical Methods in Engineering" (Prentice-Hall, Inc., Eaglewood Cliffs, New Jersey, 1961) p. 252.
17. T. R. ANTHONY and H. E. CLINE, G.E. Report No. 78CRD118 (1978).
18. R. MEHRABIAN, S. C. HSU, C. G. LEVI and S. KOU, in "Advances in Metal Processing" edited by J. J. Burke, R. Mehrabian and V. Weiss (Plenum Press, New York, 1981) p. 13.

Received 15 April
and accepted 21 September 1983